Fluorescent Probes

Rational Design of a Near-Infrared Fluorescent Probe Based on a Pyridazinone Scaffold

Tongliang Zhou,[a][‡] Lingfei Yang,[a][‡] Lei Liang,*[a] Hui Liu,[a] Yuanjun Zhu,*[b] Mengyang Shui,[b] Lan Yuan,*[c] Fengrong Xu,[a] Yan Niu,[a] Chao Wang,[a] and Ping Xu*[a]

Abstract: A class of pyridazinone derivatives as near-infrared optical probes in fluorescence microscopy images was designed. The design strategy consisted of the stepwise extension and modification of pyridazinone by expansion of the electron-donating moiety to a larger π-conjugated system and anchoring a subcellular directing group such as triphenylphosphine or morpholine. All the desired products were successfully applied in cell imaging with high subcellular colocalization. Furthermore, these fluorescent probes showed excellent performance in mouse-brain imaging.

Introduction

Fluorescence imaging for research of life processes, especially for observation of cells and tissues, has attracted extreme attention in the past decades.[1] Fluorescence probes with excellent photophysical properties and based on rhodamine, cyanine, boron–dipyrromethene (BODIPY), and other frameworks have been developed.[2] Apart from continuous efforts devoted to structural modification of probes, upgrading tissue visualization represents another urgent demand requiring suitable candidates to interpret the biological information.[3]

However, photophysical disadvantages such as short absorption/emission wavelength, small Stokes shift, and fast photobleaching often restrict applications of some conventional fluorescent probes.[4] As we know, probes with short absorption/emission wavelengths are unable to penetrate biological tissues, and this makes them inadaptable for in vivo observation. Moreover, the excitation of autofluorescence as a background of biological tissues is detrimental to the imaging effect. Furthermore, a small Stokes shift is not beneficial to the fluorescence signal owing to overlap of the excitation and emission spectra.[5] Thus, the development of novel fluorescence probes with near-infrared emission and large Stokes shifts is urgently demanded.

Pyridazinone (PY), a six-membered aromatic ring, has been manually prepared and applied as a pharmacophore in drug design.[6] In a previous report, we designed a series of full-color tunable fluorescent dyes based on pyridazinone as an electron acceptor. Preliminary application of those pyridazinone derivatives to cell imaging resulted in good cell permeability and high stability.[7] To meet the requirements for biological research, we herein used pyridazinone and its analogue, phthalazinone (PH), to construct fluorophores.

Results and Discussion

Design of Probe

We chose 6-phenylpyridazinone as an electron-withdrawing moiety to build the new fluorophores. On the basis of our previous results, the coupling of different electron-donating aromatic groups such as N,N-diethylaniline and thiophene on the 2-NH group of pyridazinone endows the products with luminescent properties. However, the fluorescent emission of the products is located in the region between 550 and 600 nm in common solvents such as DMSO. Thus, we assumed that extension of the π-conjugation system of the electron-donating moiety would enable a redshift in the absorption/emission wavelength of the fluorophore.[8] Besides, a small Stokes shift is usually the result of the rigidity of the molecular structure. Thus, an effec-

[a] Department of Medicinal Chemistry, School of Pharmaceutical Sciences, Peking University Health Science Center, Beijing, China
E-mail: leiliang@bjmu.edu.cn
pingxu@bjmu.edu.cn
[b] Department of Molecular and Cellular Pharmacology, School of Pharmaceutical Sciences, Peking University, Beijing, China
[c] Medical and Healthy Analysis Center, Peking University, Beijing, China
http://dmc.sps.bjmu.edu.cn/szdw/yjsds/139071.htm
[‡] These authors contributed equally to this paper.
📄 Supporting information for this article is available on the WWW under https://doi.org/10.1002/ejoc.201700355.

Figure 1. Design strategy for the new pyridazinone fluorescent probes.

ChemPubSoc
Europe

EurJOC
European Journal
of Organic Chemistry

Full Paper
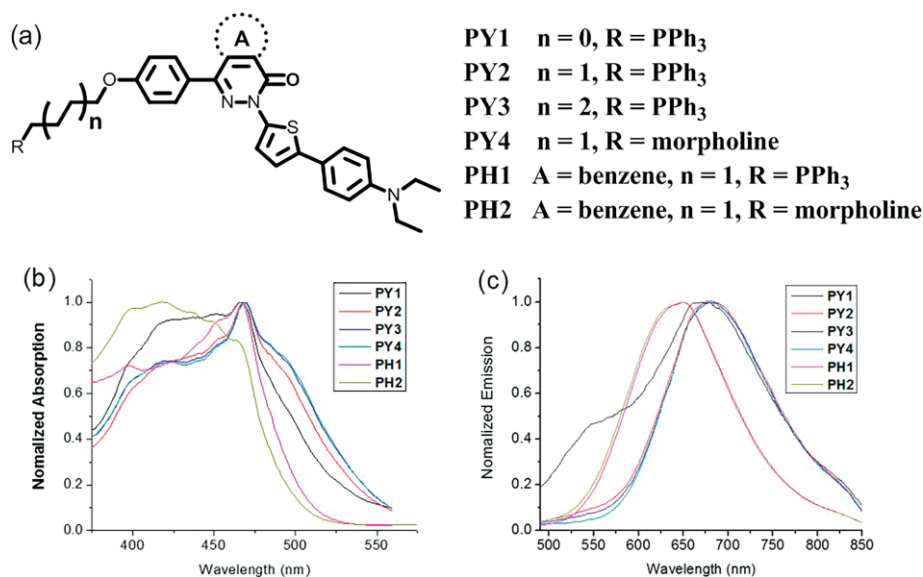
Figure 2. Structures and photophysical properties (measured in DMSO) of the novel pyridazinone-based fluorescent probes.

tive way to realize a large Stokes shift is to increase the flexibility of the fluorescent skeleton.[9] On this basis, to extend the conjugation of the molecules and to increase their vibrational flexibility, a thiophene moiety was chosen to be inserted into the original fluorophore between the pyridazinone and N,N-diethylaniline moieties (Figure 1).

Furthermore, to achieve tailor-made specificity in intracellular localization, an anchoring group on the skeleton was necessary, and thus, a 4-phenoxy group was attached to the pyridazinone. Then, the hydroxy group of the phenol moiety was alkylated with a bromoalkyl chain. Finally, carriers with lipophilic and cationic properties were installed on the alkyl chain to enhance the affinity of the fluorophores to particular organelles. For example, an alkyl chain with a terminal positively charged triphenylphosphine group was anchored to the hydroxy group of the phenol moiety, as this was expected to serve as a mitochondria-directing group, and in the same way, a morpholine group was introduced, as it was expected to serve as a lysosome-directing group (Figure 2).

Computational Details

To obtain information on the fluorophores, calculations were performed by geometrical optimization of their structures at the B3LYP/6-31G** level of density functional theory.[10] Besides, the excitation energies from the ground state to the lowest-lying excited states in the singlet manifold were also calculated.

To simplify the calculations, the methoxy group or the hydroxy group of the phenol moiety was removed. Tables 1 and 2 show the optimized geometric structures of PY and PH, and the molecular frameworks are basically composed of four aromatic rings. In sequence, the dihedral angle between the N,N-diethylaniline and thiophene moieties is 35°. However, the dihedral angle between the thiophene and pyridazinone or phthalazinone units decreases to 2 or 3°, which is indicative of its approximate planarity. Relative to that of PY (27°), the dihedral angle of phthalazinone/phenol markedly increases to 57° owing to steric effects. The optimized molecular orbitals (MOs) reflect that the delocalized electron density of the HOMO is

Table 1. HOMOs and LUMOs of the fluorescent probes as deduced by DFT calculations.

ChemPubSoc
Europe

EurJOC
European Journal
of Organic Chemistry

Full Paper

Table 2. Calculated parameters ($S_0 \to S_1$) for PY and PH.[a]

Compound	HOMO [eV]	LUMO [eV]	Excitation energy [eV]	f[b]	Composition	Dihedral angle[c] [°]
PY	−6.8500	0.1552	4.4682	0.8520	HOMO→LUMO	27/3/35
PH	−7.4393	0.1742	4.8259	0.9712	HOMO→LUMO	57/2/35

[a] Only selected excited states were considered. [b] Oscillator strength. [c] Dihedral angle: anisole/pyridazinone, thiophene/pyridazinone, thiophene/N,N-diethylaniline.

Table 3. Structure and photophysical properties of the PY and PH derivatives.[a]

Compound	A	R	ε_{max}[b]	λ^1_{max}(ex)/λ^{fl}_{max}(em)[c] (Stokes shift)	Φ_{fl}[d]	Pearson's coefficient
PY1	-	$^+$PPh$_3$	0.43	466 nm / 671 nm (205)[e]	0.136	0.78
PY2	-	$^+$PPh$_3$	1.15	468 nm / 686 nm (218)	0.302	0.91
PY3	-	$^+$PPh$_3$	1.24	469 nm / 683 nm (214)	0.235	0.95
PY4	-	N—O (morpholine)	2.42	469 nm / 681 nm (212)	0.187	0.96
PH1	⬡	$^+$PPh$_3$	1.64	466nm / 650nm (184)	0.092	0.92
PH2	⬡	N—O (morpholine)	1.55	418nm / 648nm (230)	0.078	0.87

[a] All data were measured in DMSO at 298 K. [b] Extinction coefficient in 1×10^4 m^{-1} cm^{-1}. [c] λ_{max} values of the one-photon absorption and emission spectra in nanometers. [d] Fluorescence quantum yield, with rhodamine B as a standard ($\Phi = 0.72$ in MeOH). [e] Stokes shift.

located mainly on the thiophene and N,N-diethylaniline moieties, whereas the LUMO is distributed primarily over the pyridazinone or phthalazinone unit. As the major contribution of the S_0–S_1 transition stems from the HOMO and LUMO, the results suggest that the lowest-energy electronic transition occurs predominantly through a thiophene-centered π–π* transition. The abovementioned features are also reflected in the frontier molecular orbital energy levels of PY and PH. PY shows uniquely low-lying HOMO and LUMO levels, which account for the low-energy charge-transfer transitions. This result is consistent with the measured fluorescent properties (Table 3).

Synthesis of Probes

On the basis of our previous reports, we started the synthesis of the desired compounds.[11] As depicted in Scheme 1, compound **2** was prepared by Suzuki coupling of 4-bromo-N,N-diethylaniline (**1**) with 2-thiopheneboronic acid, and then **3** was obtained by bromination of **2** with N-bromosuccinimide (NBS). Additionally, **5** was prepared by using a procedure reported by Coates.[12] Key intermediate **6** was prepared in 54 % yield by a copper(I)-catalyzed coupling reaction between **3** and **5**. Then, the hydroxy group of **6** was modified with different dibromo-

ChemPubSoc
Europe

EurJOC
European Journal
of Organic Chemistry

Full Paper
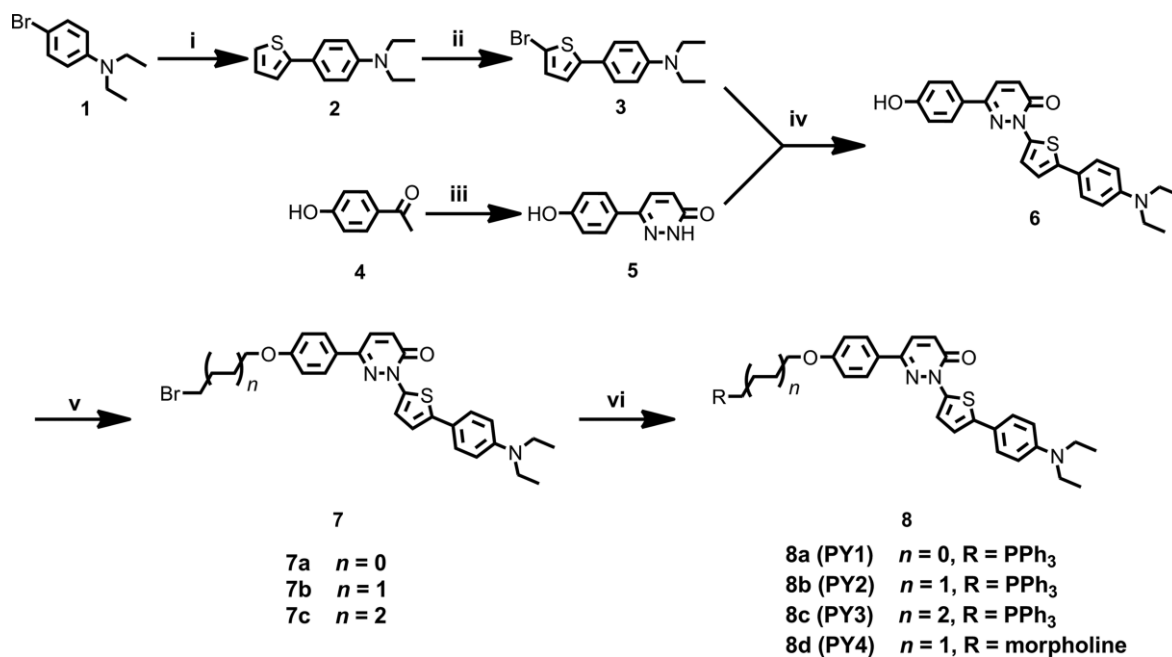
Scheme 1. Route for the synthesis of the PY derivatives. Reagents and conditions: (i) 2-thiopheneboronic acid, Pd(PPh$_3$)$_4$, K$_2$CO$_3$, toluene, EtOH, H$_2$O, 90 °C, 18 h, 42 %; (ii) NBS, THF, 12 h, 97 %; (iii) glyoxylic acid monohydrate, 100 °C, 2 h; hydrazine hydrate, H$_2$O, 100 °C, 2 h, 48 %; (iv) CuI, Cs$_2$CO$_3$, DMF, 120 °C, 28 h, 54 %; (v) dibromoalkane, K$_2$CO$_3$, MeCN, reflux, 24 h, 65–76 %; (vi) R (R = PPh$_3$ or morpholine), MeCN, reflux, 10 h, 44–85 %.
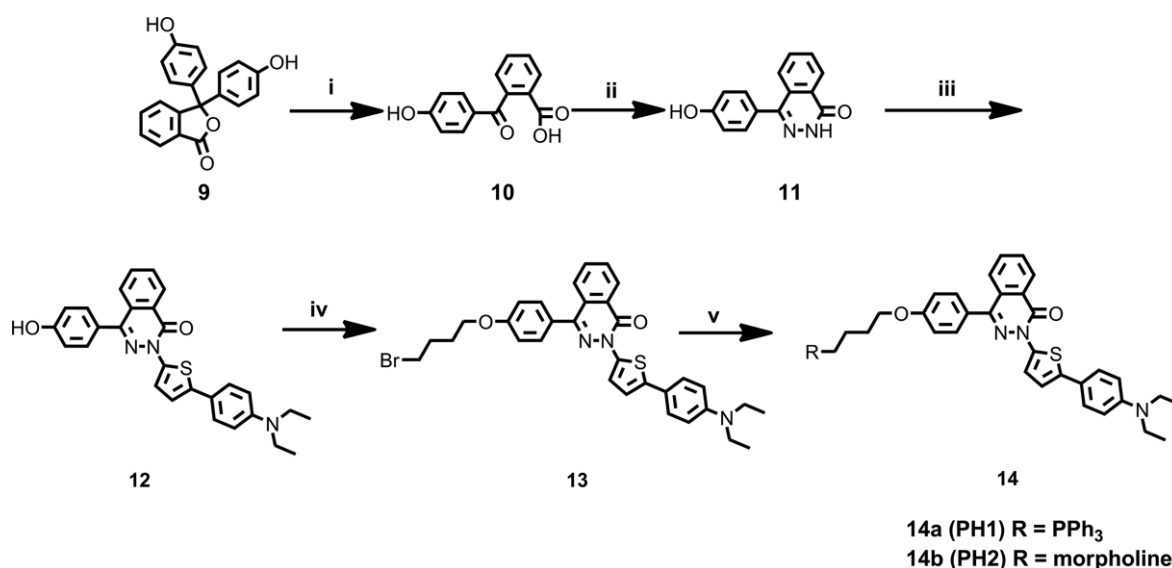
Scheme 2. Route for the synthesis of the PH derivatives. Reagents and conditions: (i) NaOH, hydroxylamine hydrochloride, H$_2$O, 80 °C; sulfuric acid, H$_2$O, 100 °C, 92 %; (ii) hydrazine hydrate, chlorobenzene, dimethylacetamide, reflux, 2 h, 82 %; (iii) 3, CuI, Cs$_2$CO$_3$, DMF, 120 °C, 24 h, 35 %; (iv) 1,4-dibromobutane, K$_2$CO$_3$, MeCN, reflux, 18 h, 68 %; (v) R (R = PPh$_3$ or morpholine), MeCN, reflux, 24 h, 78–88 %.

alkanes. Finally, the PY derivatives were obtained by substitution of the terminal bromine atom with triphenylphosphine or morpholine.

The PH derivatives were obtained in modest to good yields by a similar procedure using phenolphthalein (9) as the starting material (Scheme 2).

Photophysical Properties

Before biological evaluation, the photophysical properties of the PY and PH derivatives were measured and compiled (Figures S1 and S2 in the Supporting Information, Table 3). They generally feature a broad band around 418–469 nm with molar absorptivity in the range of 0.43×10^4 to 2.42×10^4 M^{-1} cm^{-1}, which corresponds to the $^1\pi$–π^* transition associated with the basic fluorophores.

To examine how the pyridazinone/phthalazinone moieties influence the photophysical properties, these compounds were compared: PY**2** versus PH**1** and PY**4** versus PH**2**. For instance, PY**2** shows a maximum emission at 686 nm, and this value is redshifted by 36 nm relative to the maximum emission of PH**1** (650 nm) owing to the increased electron-withdrawing ability

ChemPubSoc
Europe

EurJOC
European Journal
of Organic Chemistry

Full Paper

of the pyridazinone unit. On the other hand, insertion of a thiophene ring into the original fluorophore successfully shifts the emission wavelength of the PY and PH derivatives to the near-infrared region. Upon comparing the PY or PH derivatives, which possess identical fluorophores but different terminal modifications of the alkyl chain, we find that the appended alkyl moiety has a clear effect on the photophysical properties, probably as a result of different solubilities. The fluorescent quantum yields (Φ_{fl}) were also measured in DMSO by using rhodamine B as a reference.[13] As shown in Table 3, the PY derivatives afford moderate fluorescence quantum yields (0.136–0.302) that are higher than those of the PH derivatives (0.078 & 0.092).

Live-Cell Imaging

Live-cell imaging experiments were then performed to explore the relevance of the structures and to visualize the specific cellular behaviors of the PY and PH derivatives. Herein, triphenylphosphine was used as a mitochondrion-directing group and a commercially available mitochondrial tracker was used as a control; excellent results were obtained. Imaging of human rhabdomyosarcoma (RD) cells incubated with 2 μM PH1, PY2, and PY3 are shown in Figure 3.

All derivatives exhibit high selectivity in the mitochondrion, and the Pearson's coefficients are all above 0.90, which is indicative of excellent colocalization with mitochondrion. Furthermore, morpholine tails are shared by PY4 and PH2 for lysosomal localizations. As shown in Figure S3, both of them show excellent colocalization with Lyso-tracker in RD cells, and the Pearson's coefficients are around 0.90. Therefore, the terminal pendants of the alkyl chains determine the subcellular localization with different affinity to subcellular organelles.

Furthermore, PY1 was selected to compare the stability with Mito-Tracker Green FM, a commercial fluorescence dye. Derivative PY1 was found to show better properties against photobleaching (Figure S4). The cytotoxicities of the PY/PH derivatives were also assessed by the CCK-8 assay (Figure S5). The results indicate that all of these compounds have low cytotoxicity, even if the cells are incubated with 20 μM compounds for 24 h.

Visualization of Mouse Brain

Despite the rapid development of various fluorescence probes, few of them can be transferred successfully from cell imaging to tissue visualization. Near-infrared fluorescence probes capable of deeply penetrating biological tissues have gradually been accepted as powerful tools to observe the complexity and pathophysiology of brain tissues.[14] Thus, to establish further the utility of the PY and PH derivatives for bioimaging, these probes were employed in brain imaging. Mouse-brain slices were iso-
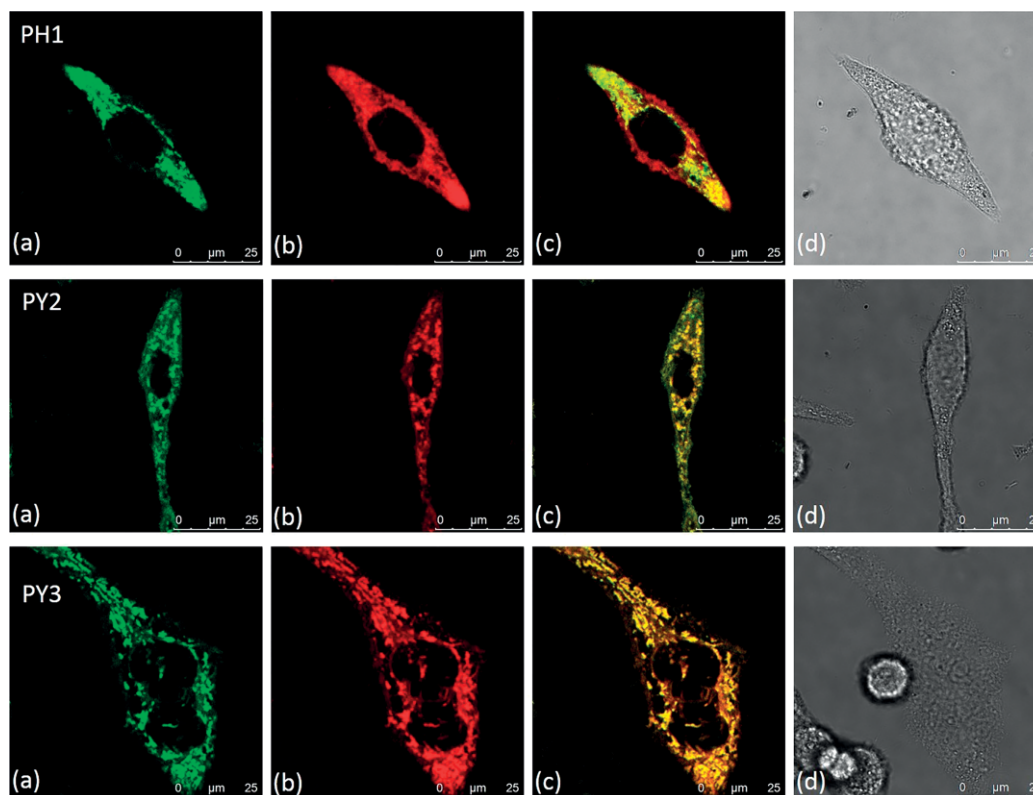
Figure 3. One-photon fluorescence colocalization images of RD cells incubated with 2 μM probes and commercial dyes. (a) Image of Mito tracker Green; (b) image of PH/PY; (c) result of merging the images shown in panels a and b. (d) Bright-field image. Images were acquired at two channels. For channel 1, with 488 nm excitation and fluorescent emission windows: green = 500–550 nm; for channel 2, with 405 nm excitation and fluorescent emission windows: red = 560–650 nm.

ChemPubSoc
Europe

EurJOC
European Journal
of Organic Chemistry

Full Paper

lated from a 2 month old mouse, and each slice was incubated with 20 μM PY**2** for 30 min at 37 °C and then imaged under a confocal laser scanning microscope. Because the structure of the brain tissue is heterogeneous, we acquired 20 images at depths of 0–200 μm to investigate the overall distribution of fluorescence. As shown in Figure 4, a significant enhancement in fluorescence intensity is observed on the surface of the brain slice (Figure 4a–c). Through observation of the stained details, we assume that the repartition of PY**2** within the tissues is mostly mitochondria colocalized (Figure 4d). Moreover, the depth of visualization approaches 200 μm for one-photon excitation (Figure 4e). Furthermore, whole mouse-brain slices, including the cerebral cortex and the central core, are observed with strong fluorescence, which indicates the potent brain-tissue-permeability of PY**2**.
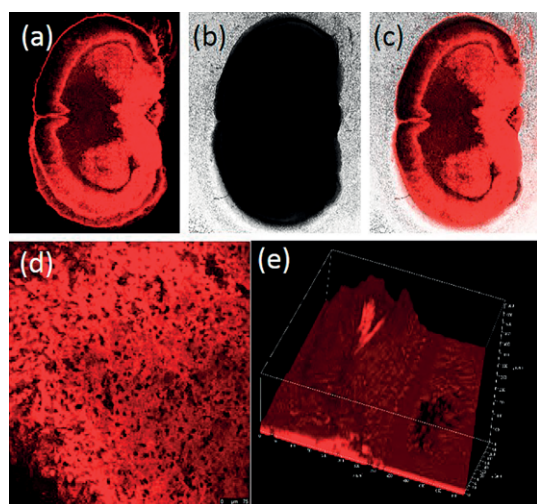
Figure 4. One-photon microscope image of a fresh mouse-brain slice (volume: 14 mm ×8 mm × 1 mm) labeled with (a) PY**2** (20 μM, 30 min) and (b) bright-field image. (c) The result of merging the image shown in panels a and b. Images were acquired at the channel using 405 nm excitation and fluorescent emission windows: red = 560–650 nm. (d) Magnification of the specific region of the mouse-brain slice. (e) Visualization depth of the mouse brain along the z axis (images were captured every 9.8 μm).

Conclusions

In summary, by rational design and computational calculations, we developed a series of near-infrared fluorescent probes for live-cell and mouse-brain imaging. A structural relationship between the photophysical properties and the biological behaviors was revealed. More importantly, the electronic states of the N-substituents of the pyridazinone moiety were found to modulate the photophysical properties of the fluorescent probes effectively, whereas the terminal pendants on the alkyl chain were found to determine the subcellular organelle selectivity. These fluorescent probes were successfully used in cell imaging with high luminescence, subcellular organelle selectivity, and mouse-brain imaging with excellent performance. These results provide important insight into the modular design of fluorescent probes and further expand the repertoire of small molecular fluorophores.

Experimental Section

General Methods: All solvents and chemicals were purchased from Alfa Aesar and J&K and were used without further purification, unless specifically mentioned. Cellular imaging trackers were purchased from Invitrogen (Life Technologies). ^{1}H NMR spectroscopy was performed by using a Bruker-400 NMR spectrometer at 400 MHz. Tetramethylsilane was used as the internal reference. Electrospray ionization (ESI) mass spectrometry was performed with a Fourier-transform ion cyclotron resonance mass spectrometer (FT-ICR, Bruker, USA). FTIR spectra were taken with a Nicolet iN10 MX Fourier-transform infrared spectrometer. The steady-state absorption spectra were attained with an Agilent 8453 UV/Vis spectrophotometer in 1 cm path-length quartz cells. Single-photon luminescence spectra were recorded by using fluorescence lifetime and a steady-state spectrophotometer (Edinburgh Instrument FLS920). Quantum yields of one-photon emission of all the synthesized compounds were measured relative to the fluorescence of rhodamine B in MeOH. Confocal fluorescent images of living cells were obtained by using a Nikon A1R-si laser scanning confocal microscope (Japan) equipped with lasers of 405/488/561/633 nm. Several lasers and channels were used to obtain the images.

Synthesis of PY1: In a round-bottomed flask, **7a** (30 mg, 0.057 mmol) and triphenylphosphine (30 mg, 0.114 mmol) were dissolved in acetonitrile (10 mL), and the mixture was heated at reflux for 10 h. The mixture was concentrated. The crude product was purified by chromatography (silica gel, dichloromethane/methanol 30:1) to afford PY**1** (21 mg, 52 %) as a red solid. M.p. ≈104–106 °C. ^{1}H NMR (400 MHz, [D$_6$]DMSO): δ = 8.08 (d, J = 9.7 Hz, 1 H, -ArH), 7.95–7.81 (m, 11 H, -ArH), 7.81–7.74 (m, 6 H, -ArH), 7.72 (d, J = 3.7 Hz, 1 H, -ArH), 7.46 (d, J = 8.2 Hz, 2 H, -ArH), 7.22 (d, J = 9.7 Hz, 1 H, -ArH), 7.18 (d, J = 3.7 Hz, 1 H, -ArH), 6.77 (d, J = 8.2 Hz, 2 H, -ArH), 6.68 (d, J = 8.3 Hz, 2 H, -ArH), 4.46–4.34 (m, 2 H, -CH$_2$), 4.33–4.22 (m, 2 H, -CH$_2$), 3.36 [q, J = 6.6 Hz, 4 H, -N(CH$_2$)$_2$], 1.10 (t, J = 6.8 Hz, 6 H, -2CH$_3$) ppm. ^{13}C NMR (101 MHz, [D$_6$]DMSO): δ = 158.83 (-C-OCH$_2$), 156.77 (-C=O), 147.57 (-ArC), 144.42 (-ArC), 141.06 (-ArC), 139.85 (-ArC), 135.38 (d, J = 2.7 Hz, -PPh_3), 134.19 (d, J = 10.4 Hz, -PPh_3), 130.58 (d, J = 12.7 Hz, -PPh_3), 130.08 (-ArC), 128.32 (-ArC), 127.59 (-ArC), 126.87 (-ArC), 120.67 (-ArC), 119.28 (-ArC), 119.17 (-ArC), 119.07 (d, J = 86.7 Hz, -PPh_3), 115.04 (-ArC), 112.19 (-ArC), 61.78 (d, J = 5.3 Hz, -OCH$_2$), 44.16 (-CH_2CH$_3$), 29.52 (d, J = 5.6 Hz, -CH_2PPh$_3$), 12.70 (-CH$_2$$CH_3$) ppm. HRMS (ESI): calcd. for C$_{44}$H$_{41}$N$_3$O$_2$PS 706.2652 [M]$^+$; found 706.2593.

Synthesis PY2: Following the procedure outlined for the synthesis of PY**1**, **7b** was treated with triphenylphosphine. Compound PY**2** was obtained as a red solid in 70 % yield. M.p. ≈102–104 °C. ^{1}H NMR (400 MHz, [D$_6$]DMSO): δ = 8.12 (d, J = 9.8 Hz, 1 H, -ArH), 7.97 (d, J = 8.4 Hz, 2 H, -ArH), 7.92–7.88 (m, 3 H, -ArH), 7.86–7.80 (m, 6 H, -ArH), 7.79–7.77 (m, 6 H, -ArH), 7.73 (d, J = 4 Hz, 1 H, -ArH), 7.45 (d, J = 8.3 Hz, 2 H, -ArH), 7.21 (d, J = 9.7 Hz, 1 H, -ArH), 7.18 (d, J = 3.9 Hz, 1 H, -ArH), 7.04 (d, J = 8.4 Hz, 2 H, -ArH), 6.68 (d, J = 8.4 Hz, 2 H, -ArH), 4.12 (t, J = 5.7 Hz, 2 H, -OCH$_2$), 3.77–3.68 (m, 2 H, -CH$_2$), 3.34 [q, J = 7.2 Hz, 4 H, -N(CH$_2$)$_2$], 2.02–1.90 (m, 2 H, -CH$_2$), 1.78–1.66 (m, 2 H, -CH$_2$), 1.08 (t, J = 6.9 Hz, 6 H, -2CH$_3$) ppm. ^{13}C NMR (101 MHz, [D$_6$]DMSO): δ = 159.90 (-C-OCH$_2$), 156.25 (-C=O), 147.02 (-ArC), 144.16 (-ArC), 140.48 (-ArC), 139.36 (-ArC), 134.88 (d, J = 2.0 Hz, -PPh_3), 133.57 (d, J = 10.2 Hz, -PPh_3), 130.64 (-ArC), 130.21 (d, J = 12.5 Hz, -PPh_3), 129.63 (-ArC), 127.74 (-ArC), 126.34 (-ArC), 126.13 (-ArC), 120.19 (-ArC), 118.70 (-ArC), 118.65 (-ArC), 118.44 (d, J = 85.7 Hz, -PPh_3), 114.97 (-ArC), 111.66 (-ArC), 66.23 (-OCH$_2$), 43.64 (-CH_2CH$_3$), 29.04 (d, J = 17.0 Hz, -CH_2PPh$_3$), 19.75 (d, J = 50.1 Hz, -OCH$_2$$CH_2$), 18.44 (d, J = 4.0 Hz, -CH_2CH$_2$PPh$_3$), 12.68 (-CH$_2$$CH_3$) ppm. HRMS (ESI): calcd. for C$_{46}$H$_{45}$N$_3$O$_2$PS 734.2965 [M]$^+$; found 734.2903.

ChemPubSoc
Europe

EurJOC
European Journal
of Organic Chemistry

Full Paper

Synthesis of PY3: Following the procedure outlined for the synthesis of PY**1**, **7c** was treated with triphenylphosphine. Compound PY**3** was obtained as a red solid in 44 % yield. M.p. ≈102–104 °C. ^{1}H NMR (400 MHz, CDCl$_3$): δ = 7.93–7.74 (m, 12 H, -ArH), 7.73–7.62 (m, 7 H, -ArH), 7.50 (d, J = 8.4 Hz, 2 H, -ArH), 7.08 (d, J = 9.6 Hz, 1 H, -ArH), 7.03 (d, J = 3.7 Hz, 1 H, -ArH), 6.96 (d, J = 8.4 Hz, 2 H, -ArH), 6.67 (d, J = 8.2 Hz, 2 H, -ArH), 3.99 (t, J = 5.8 Hz, 2 H, -OCH$_2$), 3.86 (t, J = 6.6 Hz, 2 H, -CH$_2$), 3.38 [q, J = 6.9 Hz, 4 H, -N(CH$_2$)$_2$], 1.81–1.73 (m, 4 H, -2CH$_2$), 1.63–1.69 (m, 2 H, -CH$_2$), 1.63–1.69 (m, 4 H, -CH$_2$), 1.18 (t, J = 6.9 Hz, 6 H, -2CH$_3$) ppm. ^{13}C NMR (101 MHz, CDCl$_3$): δ = 160.69 (-C-OCH$_2$), 157.15 (-C=O), 147.49 (-ArC), 144.58 (-ArC), 141.84 (-ArC), 140.71 (-ArC), 135.08 (d, J = 3.0 Hz, -PPh_3), 133.85 (d, J = 10.1 Hz, -PPh_3), 130.60 (-ArC), 130.59 (d, J = 12.6 Hz, -PPh_3), 128.85 (-ArC), 128.72 (-ArC), 127.79 (-ArC), 127.01 (-ArC), 126.72 (-ArC), 119.35 (-ArC), 118.92 (-ArC), 118.61 (d, J = 86.2 Hz, -PPh_3), 115.16, 111.97, 68.04 (-OCH$_2$), 44.54 (-CH$_2$CH$_3$), 30.11 [d, J = 15.8 Hz, -CH$_2$(CH$_2$)$_2$PPh$_3$], 29.81 (-CH$_2$PPh$_3$), 28.88 (-OCH$_2$CH$_2$), 25.74 [-O(CH$_2$)$_2$$CH_2$], 22.79 (d, J = 3.06 Hz, -CH$_2$CH$_2$PPh$_3$), 12.68 (-CH$_2$$CH_3$) ppm. HRMS (ESI): calcd. for C$_{48}$H$_{49}$N$_3$O$_2$PS 762.3278 [M]$^+$; found 762.3206.

Synthesis of PY4: In a round-bottomed flask, **7b** (80 mg, 0.14 mmol), morpholine (38 mg, 0.43 mmol), and potassium carbonate (60 mg, 0.43 mmol) were mixed in acetonitrile (10 mL), and the mixture was heated at refluxed for 10 h. After cooling, the mixture was filtered, and the filtrate was concentrated under reduced pressure. The residue was purified by chromatography (silica gel, dichloromethane/methanol 20:1) to afford PY**4** (68 mg, 85 %) as a red solid. M.p. ≈114–116 °C. ^{1}H NMR (400 MHz, CDCl$_3$): δ = 7.83 (d, J = 6.1 Hz, 2 H, -ArH), 7.81 (s, 1 H, -ArH), 7.65 (d, J = 9.7 Hz, 1 H, -ArH), 7.51 (d, J = 8.7 Hz, 2 H, -ArH), 7.11 (d, J = 9.6 Hz, 1 H, -ArH), 7.05 (d, J = 4.1 Hz, 1 H, -ArH), 6.99 (d, J = 8.7 Hz, 2 H, -ArH), 6.69 (d, J = 8.8 Hz, 2 H, -ArH), 4.05 (t, J = 6.1 Hz, 2 H, -OCH$_2$), 3.77 (t, J = 6.1 Hz, 4 H, -2CH$_2$), 3.39 [q, J = 7 Hz, 4 H, -N(CH$_2$CH$_3$)$_2$], 2.62–2.42 (m, 6 H, -3CH$_2$), 1.91–1.82 (m, 2 H, -CH$_2$), 1.80–1.67 (m, 2 H, -CH$_2$), 1.19 (t, J = 7 Hz, 6 H, -2CH$_3$) ppm. ^{13}C NMR (101 MHz, CDCl$_3$): δ = 160.60 (-C-OCH$_2$), 157.15 (-C=O), 147.49 (-ArC), 144.47 (-ArC), 141.89 (-ArC), 140.68 (-ArC), 130.65 (-ArC), 128.60 (-ArC), 127.81 (-ArC), 127.04 (-ArC), 126.94 (-ArC), 121.56 (-ArC), 119.40 (-ArC), 118.95 (-ArC), 115.08 (-ArC), 111.95 (-ArC), 67.92 (-OCH$_2$), 66.82 (-OCH$_2$CH$_2$N), 58.66 (-NCH$_2$CH$_2$O), 53.71 [-NCH$_2$(CH$_2$)$_3$O], 44.56 (-CH$_2$CH$_3$), 27.20 [-N(CH$_2$)$_2$$CH_2CH_2$O], 22.98 [-NCH$_2CH_2$(CH$_2$)$_2$O], 12.76 (-CH$_2$$CH_3$) ppm. HRMS (ESI): calcd. for C$_{32}$H$_{39}$N$_4$O$_3$S 559.2743 [M + H]$^+$; found 559.2692.

Synthesis of PH1: Following the procedure outlined for the synthesis of PY**4**, **13** was treated with triphenylphosphine. Compound PH**1** was obtained as a red solid in 78 % yield. M.p. ≈115–117 °C. ^{1}H NMR (400 MHz, CDCl$_3$): δ = 8.57 (d, J = 7.7 Hz, 1 H, -ArH), 7.87–7.73 (m, 12 H, -ArH), 7.710–7.63 (m, 7 H, -ArH), 7.57 (d, J = 8.5 Hz, 2 H, -ArH), 7.46 (d, J = 7.9 Hz, 2 H, -ArH), 7.00 (m, 3 H, -ArH), 6.65 (d, J = 7.6 Hz, 2 H, -ArH), 4.20 (t, J = 5.7 Hz, 2 H, -OCH$_2$), 4.03–3.91 (m, 2 H, -CH$_2$), 3.36 [q, J = 6.7 Hz, 4 H, -N(CH$_2$)$_2$], 2.31–2.20 (m, 2 H, -CH$_2$), 1.94–1.85 (m, 2 H, -CH$_2$), 1.16 (t, J = 6.9 Hz, 6 H, -2CH$_3$) ppm. ^{13}C NMR (101 MHz, CDCl$_3$): δ = 159.85 (-C-OCH$_2$), 156.59 (-C=O), 147.78 (-ArC), 147.22 (-ArC), 140.95 (-ArC), 140.66 (-ArC), 135.10 (d, J = 2.9 Hz, -PPh_3), 133.79 (d, J = 9.9 Hz, -PPh_3), 133.09 (-ArC), 131.89 (-ArC), 131.11 (-ArC), 130.96 (-ArC), 130.57 (d, J = 12.4 Hz, -PPh_3), 128.86 (-ArC), 128.38 (-ArC), 128.21 (-ArC), 127.66 (-ArC), 127.27 (-ArC), 127.17 (-ArC), 126.82 (-ArC), 118.38 (d, J = 85.9 Hz, -PPh_3), 118.29 (-ArC), 114.77 (-ArC), 111.92 (-ArC), 66.78 (-OCH$_2$), 44.45 (-CH$_2$CH$_3$), 29.34 (d, J = 16.8 Hz, -CH$_2$PPh$_3$), 22.15 (d, J = 50.7 Hz, -OCH$_2$CH$_2$), 19.41 (d, J = 3.6 Hz, -CH$_2$CH$_2$PPh$_3$), 12.69 (-CH$_2$$CH_3$) ppm. HRMS (ESI): calcd. for C$_{50}$H$_{47}$N$_3$O$_2$PS 784.3121 [M]$^+$; found 784.3059.

Synthesis of PH2: Following the procedure outlined for the synthesis of PY**4**, **13** was treated with morpholine and potassium carbonate. Compound PH**2** was obtained as an orange-red oil in 88 % yield. ^{1}H NMR (400 MHz, CDCl$_3$): δ = 8.56 (d, J = 7.5 Hz, 1 H, -ArH), 7.82–7.72 (m, 2 H, -ArH), 7.66–7.72 (m, 2 H, -ArH), 7.58 (d, J = 8.5 Hz, 2 H, -ArH), 7.48 (d, J = 8.8 Hz, 2 H, -ArH), 6.98–7.06 (m, 3 H, -ArH), 6.65 (d, J = 8.8 Hz, 2 H, -ArH), 4.04 (t, J = 6.2 Hz, 2 H, -OCH$_2$), 3.73 (t, J = 4.5 Hz, 4 H, -2CH$_2$), 3.35 [q, J = 7 Hz, 4 H, -N(CH$_2$CH$_3$)$_2$], 2.53–2.45 (m, 4 H, -2CH$_2$), 2.43 (t, J = 7.5 Hz, 2 H, -CH$_2$), 1.90–1.80 (m, 2 H, -CH$_2$), 1.76–1.65 (m, 2 H, -CH$_2$), 1.16 (t, J = 7 Hz, 6 H, -2CH$_3$) ppm. ^{13}C NMR (101 MHz, CDCl$_3$): δ = 160.05 (-C-OCH$_2$), 156.43 (-C=O), 147.66 (-ArC), 147.16 (-ArC), 140.55 (-ArC), 140.43 (-ArC), 132.86 (-ArC), 131.71 (-ArC), 131.01 (-ArC), 128.81 (-ArC), 128.32 (-ArC), 128.16 (-ArC), 127.57 (-ArC), 127.14 (-ArC), 126.74 (-ArC), 121.73 (-ArC), 118.46 (-ArC), 118.20 (-ArC), 114.59 (-ArC), 111.87 (-ArC), 67.83 (-OCH$_2$), 66.92 (-OCH$_2$CH$_2$N), 58.59 (-NCH$_2$CH$_2$O), 53.70 [-NCH$_2$(CH$_2$)$_3$O], 44.40 (-CH$_2$CH$_3$), 27.16 [-N(CH$_2$)$_2$$CH_2CH_2$O], 23.05 [-NCH$_2CH_2$(CH$_2$)$_2$O], 12.67 (-CH$_2$$CH_3$) ppm. HRMS (ESI): calcd. for C$_{36}$H$_{41}$N$_4$O$_3$S 609.2899 [M + H]$^+$; found 609.2879.

Determination of the Fluorescence Quantum Yield of the PY and PH Derivatives: The quantum yields of one-photon emission of the synthesized PY and PH derivatives were measured with rhodamine B (RhB, Φ = 0.72, dissolved in MeOH) as a reference. The one-photon fluorescence measurements were performed in 1 cm quartz cells with 1 μM compound in DMSO or CH$_2$Cl$_2$ with a fluorescence lifetime and steady-state spectrophotometer (Edinburgh Instrument FLS920) equipped with a 450 W Xenon light and 2.5 × 2.5 slits. The values of fluorescence quantum yield, Φ (sample), were calculated according to the following equation:[15]

$$\Phi_{sample} = \Phi_{ref} \cdot \frac{OD_{ref} \cdot I_{sample} \cdot d_{sample}^2}{OD_{sample} \cdot I_{ref} \cdot d_{ref}^2}$$

in which Φ_{ref} is the value of the fluorescence quantum yield of the reference (Φ_{RhB} = 0.72),[16] I is the integrated emission intensity, OD is the optical density at the excitation wavelength, and d is the refractive index of the solvent (d_{DMSO} = 1.478, $d_{CH_2Cl_2}$ = 1.444, d_{H_2O} = 1.333, d_{MeOH} = 1.329).

Cell Culture: All cells were incubated in complete medium [Dulbecco's modified Eagle's Medium, supplemented with 10 % fetal bovine serum (FBS) and 1 % penicillin–streptomycin] at 37 °C under an atmosphere containing 5 % CO$_2$. For imaging, RD cells were grown in poly-D-lysine-coated dishes and were incubated in complete medium (2 mL) for 24 h. Cells were washed with phosphate-buffered saline (PBS), and stocked dyes (2 mM in DMSO) were added to obtain a final concentration of 2 μM. The treated cells were incubated for 30 min in the dark at 37 °C. A few minutes prior to confocal imaging, cells were washed with PBS (2×). A confocal laser scanning microscope (A1R-si, Nikon, Japan) was used to obtain images. Cells were imaged by the fluorescence mode with a 40× immersion lens with the following parameters: laser power 3 %; pinhole 1.0 au; excitation wavelength 405, 488, 561, or 633 nm; resolution 512 × 512; and a scan speed of 0.5 frames s^{-1}.

Colocalization Assay: RD cells were placed onto 0.1 mM poly-D-lysine-coated glasses in complete medium, and the cells were incubated for 24 h. A stock solution of PY or PH in chromatographic grade, anhydrous DMSO was prepared as 2 mM. The solution was diluted to a final concentration of 2 μM by adding complete growth medium. Stock solutions of Mito-Tracker Green FM, Lyso-Tracker Green DND-26 were prepared as 1 mM, and the stock solution was diluted to the working concentration in complete medium (100 nM). After incubating for 30 min, cells were washed with PBS buffer (2×) before the confocal experiments. Images were taken under condi-

tions as follows: 40× immersion lens with a resolution of 512 × 512 and a speed of 0.5 frames s⁻¹, suitable excitation wavelength and detector slit for PY or PH with respect to their fluorescence wavelength, 3 % laser power for PY or PH samples, and 2 % laser power for Mito Tracker and Lyso Tracker. The Pearson's Coefficient was calculated by Image J colocalizing the red in the green.

Visualization of Mouse Brain: The mice were firstly anesthetized with chloral hydrate (500 mg kg⁻¹, intraperitoneal injection) until there was no righting reflex. The thoracic cavity was exposed by a midline incision. The right auricle was cut open and perfused with cold normal saline (10 mL) from the left ventricle. Subsequently, the brains were dissected rapidly and cut into 0.5 mm coronal slices. Mouse-brain slices were treated with 20 μM PY**2** for 30 min at 37 °C and were then washed with prewarmed PBS buffer before photoirradiation at 405 nm. One-photon fluorescence microscopy images were obtained with a Leica TCS SP8 confocal laser-scanning microscope (CLSM, Heidelberg, Germany). The microscopy settings were as follows: 16× immersion lens objective, resolution of 512 × 512, 405 nm excitation wavelength, red silts for PY**2**, 10 % laser power (10 mW). A total of 20 images at depths of 0–200 μm were acquired to investigate the overall distribution of fluorescence.

Photostability in Cells: Photostability comparison of the PY/PH derivatives and commercial trackers as subcellular organelles makers were conducted in RD cells. As shown in Figure S4, both rows show one-photon confocal microscopy images of RD cells costained with selected commercial Mito-Tracker Green FM (green) and PY**1** (red). The images were taken at 0, 60, 180, 360 and 480 s under successive irradiation. All images were obtained under the same conditions.

Cytotoxicity Assay: The cytotoxicity assays were conducted according to the literature.[17] RD cells were seeded in flat-bottomed 96-well plates, 10⁴ cells well⁻¹, with complete culture medium (200 μL) in the dark for 24 h. After washing with PBS (3 × 200 μL), the cells were incubated with 2/5/10/20/40 μM of the PY/PH derivatives. All stock solutions were prepared in DMSO and were diluted with complete medium, and the final DMSO concentrations were less than 0.1 %. The cells were cultured for 24 h and were then washed with PBS (3 × 200 μL). Cell Counting Kit-8 (CCK-8) solution (10 μL) and PBS (90 μL) were simultaneously added per well. After 2 h, the absorbance at 450 nm was read by a 96-well plate reader. The viability of RD cells was calculated by the following equation:

$$CV = \frac{(As-Ab)}{(Ac-Ab)} \times 100\ \%$$

in which CV is the cell viability, and As, Ac, and Ab are the absorbances of the cells containing the PY/PH derivatives, cell control (0 μM PY/PH), and blank control (wells containing no cells or PY/PH), respectively.

Supporting Information (see footnote on the first page of this article): Synthesis of intermediates **2**–**13**; computational results; and ¹H NMR, ¹³C NMR, fluorescence absorption, and emission spectra of the probes in different solvents.

Note: The authors declare no competing financial interest.

Acknowledgments

[1] a) W. Rettig, B. Strehmel, S. Schrader, H. Seifert (Eds.), *Applied Fluorescence in Chemistry, Biology, and Medicine*, Springer, New York, **1999**; b) J. J. Lavigne, E. V. Anslyn, *Angew. Chem. Int. Ed.* **2001**, *40*, 3118–3130; *Angew. Chem.* **2001**, *113*, 3212–3225; c) J. Rao, A. Dragulescu-Andrasi, H. Yao, *Curr. Opin. Biotechnol.* **2007**, *18*, 17–25; d) J. Zhang, R. E. Campbell, A. Y. Ting, R. Y. Tsien, *Nat. Rev. Mol. Cell. Biol.* **2002**, *3*, 906–918.

[2] a) B. N. G. Giepmans, S. R. Adams, M. H. Ellisman, R. Y. Tsien, *Science* **2006**, *312*, 217–224; b) M. Vendrell, D. Zhai, J. Cheng Er, Y.-T. Chang, *Chem. Rev.* **2012**, *112*, 4391–4420; c) G. Lukinavičius, K. Umezawa, N. Olivier, A. Honigmann, G. Yang, T. Plass, V. Mueller, L. Reymond, I. R. Corrêa Jr., Z.-G. Luo, C. Schultz, E. A. Lemke, P. Heppenstall, C. Eggeling, S. Manley, K. Johnsson, *Nat. Chem.* **2013**, *5*, 132–139.

[3] a) M. A. Paley, J. A. Prescher, *MedChemComm* **2014**, *5*, 255–267; b) J. A. Prescher, C. H. Contag, *Curr. Opin. Chem. Biol.* **2014**, *18*, 80–89.

[4] a) M. A. Haidekker, E. A. Theodorakis, *Org. Biomol. Chem.* **2007**, *5*, 1669–1678; b) J. Cody, S. Mandal, L. Yang, C. J. Fahrni, *J. Am. Chem. Soc.* **2008**, *130*, 13023–13032.

[5] J. R. Lakowicz, *Principles of Fluorescence Spectroscopy*, 2nd ed., Kluwer Academic, New York, **1999**.

[6] a) A. D. Goldberg, J. Nicklas, S. Goldstein, *Am. J. Cardiol.* **1991**, *68*, 631–636; b) J. A. Barrett, R. H. Meacham, M. F. Kelley Jr., W. F. Graney, M. H. Perrone, *Cardiovasc. Drug Rev.* **1990**, *8*, 323–338; c) R. F. Kauffman, D. W. Robertson, R. B. Franklin, G. E. Sandusky Jr., F. Dies, J. L. McNay, J. S. Hayes, *Cardiovasc. Drug Rev.* **1990**, *8*, 303–322; d) R. Hudkins, R. Raddatz, M. Tao, J. Mathiasen, L. Aimone, N. Becknell, C. Prouty, L. Knutsen, M. Yazdanian, G. Moachon, M. Ator, J. Mallamo, M. Marino, E. Bacon, M. Williams, *J. Med. Chem.* **2011**, *54*, 4781–4792; e) D. Ukena, C. Rentz, C. Reiber, G. W. Sybrecht, *Resp. Med.* **1995**, *89*, 441–444; f) S. Ovais, K. Javed, S. Yaseen, R. Bashir, P. Rathore, R. Yaseen, A. D. Hameed, M. Samim, *Eur. J. Med. Chem.* **2013**, *67*, 352–358; g) O. U. Tan, K. Ozadali, P. Yogeeswari, D. Sriram, A. Balkan, *Med. Chem. Res.* **2012**, *21*, 2388–2394.

[7] a) L. Liang, W. Wang, J. Wu, F. Xu, Y. Niu, B. Xu, P. Xu, *Chem. Eur. J.* **2013**, *19*, 13774–13782; b) L. Yang, Y. Zhu, M. Shui, T. Zhou, Y. Cai, W. Wang, F. Xu, Y. Niu, C. Wang, J.-L. Zhang, P. Xu, L. Yuan, L. Liang, *Chem. Eur. J.* **2016**, *22*, 12363–12370.

[8] a) X. Zhang, L. Chi, S. Ji, Y. Wu, P. Song, K. Han, H. Guo, T. D. James, J. Zhao, *J. Am. Chem. Soc.* **2009**, *131*, 17452–17463; b) S. Ji, J. Yang, Q. Yang, S. Liu, M. Chen, J. Zhao, *J. Org. Chem.* **2009**, *74*, 4855–4865.

[9] a) J. Y. Shao, S. M. Ji, X. L. Li, J. Z. Zhao, F. Zhou, H. M. Guo, *Eur. J. Org. Chem.* **2011**, 6100–6109; b) Z. Chamas, E. Marchi, A. Modelli, Y. Fort, P. Ceroni, V. Mamane, *Eur. J. Org. Chem.* **2013**, 2316–2324.

[10] a) E. Runge, E. K. U. Gross, *Phys. Rev. Lett.* **1984**, *52*, 997–1000; b) A. D. Becke, *J. Chem. Phys.* **1993**, *98*, 5648–5652; c) A. D. Laurent, D. Jacquemin, *Int. J. Quantum Chem.* **2013**, *113*, 2019–2039.

[11] a) L. Liang, G. Yang, W. Wang, F. Xu, Y. Niu, Q. Sun, P. Xu, *Adv. Synth. Catal.* **2013**, *355*, 1284–1290; b) L. Liang, G. Yang, F. Xu, Y. Niu, Q. Sun, P. Xu, *Eur. J. Org. Chem.* **2013**, 6130–6136; c) L. Liang, W. Wang, F. Xu, Y. Niu, Q. Sun, P. Xu, *Org. Lett.* **2013**, *15*, 2770–2773; d) W. Wang, L. Liang, F. Xu, W. Huang, Y. Niu, Q. Sun, P. Xu, *Eur. J. Org. Chem.* **2014**, 6863–6867.

[12] W. J. Coates, A. McKillop, *Synthesis* **1993**, *3*, 334–342.

[13] a) C. Xu, W. W. Webb, *J. Opt. Soc. Am. B* **1996**, *13*, 481–491; b) G. A. Crosby, J. N. Demas, *J. Phys. Chem.* **1971**, *75*, 991–1024.

[14] M. Cui, M. Ono, H. Watanabe, H. Kimura, B. Liu, H. Saji, *J. Am. Chem. Soc.* **2014**, *136*, 3388–3394.

[15] T. Karstens, K. Kobs, *J. Phys. Chem.* **1980**, *84*, 1871–1872.

[16] See ref.[13b]

[17] M. Ishiyama, Y. Miyazono, K. Sasamoto, Y. Ohkura, K. Ueno, *Talanta* **1997**, *44*, 1299–1305.